The International Journal of Advanced Manufacturing Technology (2023) 124:1183–1198
https://doi.org/10.1007/s00170-022-10536-1

ORIGINAL ARTICLE

Color appearance in rotational material jetting

Ali Payami Golhin[1] · **Aditya Suneel Sole**[2] · **Are Strandlie**[1]

Received: 16 June 2022 / Accepted: 11 November 2022 / Published online: 29 November 2022

Abstract
Material jetting (MJT) is a recognized additive manufacturing (AM) method to combine various materials and create a wide range of designed appearances. However, the measured color of MJT objects is frequently different from the color provided in the printer software. As a result, estimating the color quality and the measured color attributes of an object before printing is vital for accurate color reproduction. This study investigates the color variation based on the texture in an object 3D-printed using the MJT method on a rotary tray. The novel radial shape of the rotary tray build platform and variation in the layers structure were targeted as the main factors that can increase the uncertainty in accurate color reproduction. The influence of the PolyJet printer setup has been examined by thickness variation of the colored layers, location on the tray (swath selection), ink color, and finish type between layers. Color quality was assessed by comparing the produced object color by calculating spectral and colorimetric differences. Spearman rank correlation coefficient and principal component analysis (PCA) methods were used to analyze the direct or indirect influence of independent categorical factors on the measured color variables. Based on the studied parameters, switching swathes did not fail printer objects for industrial color matching. In contrast, a thickness variation as small as 0.5 mm could cause CIEDE2000 above 5 for most models, resulting in unnatural color reproduction. Color differences in most objects might be discernible to inexperienced observers, depending on the 3D printing parameters.

Keywords 3D printing · Material jetting · PolyJet · Color accuracy · Surface texture · Appearance

1 Introduction

The rapid development of office 3D printers offers a broader range of innovative designs that were previously impossible to produce using traditional manufacturing methods. Vat photopolymerization (VPP) [1] and material jetting (MJT) [2] are two examples of current AM methods that have been adapted to the personal 3D printing market. It opens new avenues for the economy and society due to its rapid development in recent years. While material jetting has made significant advances in the enhancement of surface roughness [3], the technology has yet to catch up with the development of fused filament fabrication (FFF) in terms of personal applications [4, 5].

✉ Ali Payami Golhin
payami.ag@gmail.com; ali.p.golhin@ntnu.no

[1] Department of Manufacturing and Civil Engineering, Norwegian University of Science and Technology, 2815 Gjøvik, Norway

[2] Department of Computer Science, Norwegian University of Science and Technology, 2815 Gjøvik, Norway

Prototyping is the primary purpose of personal 3D printers. Data from over 10,000 3D printers shows that they are mostly used for prototypes, hobbies, gadgets, art/fashion, and scale models [6]. This means that rather than mechanical or thermal capabilities, the quality of 3D-printed items is judged primarily based on their tactile and appearance perception. Instrumental color measurement is an indirect practical method of analyzing a product based on its appearance to evaluate the processing performance and quality of manufactured products. However, visual color assessments and color perception are qualitative, subjective, and controversial. It has become an industry concept of quality control to determine, among other things, color strength, color difference, match prediction, shade sorting, and whiteness measuring [7]. A spectroradiometer is a valuable tool for measuring light over complex shapes and designs, as it measures both wavelength and intensity for radiance, luminance, and chromaticity remotely.

The reproduction of appearance is one of the most significant aspects of 3D printing using MJT technology [8]. Since 2014, several companies, including 3D systems, MCOR-technology, HP Multi Jet Fusion (MJF), and Stratasys,

have introduced multicolor 3D printers based on powder, paper, or plastic [9]. Currently, color reproduction systems use halftoning techniques, which combine different inks spatially at the surface of an object to create colors. As a result, the object exhibits a variety of artifacts, particularly when viewed from a closer distance [8]. Y. Cheng et al. [10] prepared photocurable resins for MJT and colored the resin with CMYKW colors to achieve full-color printing using a homemade MJT printer. They developed mechanical mechanisms, automatic print head alignment algorithms, leveling mechanisms, and color dithering methods to improve color consistency. Using a custom MJT printer for 3D printing, V. Babaei et al. proposed a method for reproducing color using a 3D printing process. They create colors by combining inks with different thicknesses inside the volume of the object by 3D color contouring, which was inspired by the inherent ability of 3D printers to layer different materials over one another. Most of these studies, however, focused on the conventional movement of the build platform in MJT 3D printers.

Rotational 3D printing is currently being introduced to help reduce the size and complexity of 3D printers without using large robot arms. PolyJet® 3D printing, developed by Stratasys, is a promising MJT method that utilizes a rotary tray to create realistic-looking colored parts, such as physical replicas of biological structures, prototype samples, educational models, and artistic designs [11]. Office 3D printers have recently repurposed MJT for the personal 3D printing market. The PolyJet system builds three-dimensional objects by jetting fine droplets of photopolymer in CMYKW (cyan, magenta, yellow, black, and white), solidifying when exposed to ultraviolet light [11]. Thermoplastics and elastomers are used more frequently than photopolymers in some production environments, yet they can simulate these materials mechanically, thermally, and visually [12]. As a result of the high-resolution 3D printers available in MJT, it is now possible to print single objects with numerous colors and various surface properties, including a variety of color shades, anisotropic reflectance (AR), gloss, halftone patterns, and goniochromatic effects [11].

While the dimension accuracy and surface finishing in the manufactured objects represent high manufacturing quality, printed objects have a measured color that often differs from the selected color in the printer software. Currently, limited studies have been conducted on accurate color reproduction methods for various color 3D printing materials. Compared to color studies on AM processes with color reproduction capability, such as FDM [13–15] as the dominant AM technique, materials jetting allows for greater control over the color reproduction of 3D-printed items. For instance, X. Wei et al. [16] studied the significant-finish effects type on measured color, as well as the interaction effects of finish type and specified color. L. Zheng et al. [17] characterized the achievable range of color by comparing the gamut of PolyJet color 3D printing and ink-jet printing on a paper surface. Effects of the number of printing layers, hue, brightness, saturation, and chromatic aberration have been studied by C. Li et al. [18]. The colorimetric characterization of 3D printers using highly translucent printing materials was addressed by c. A. Arikan et al. [19]. In another study, O. Elek et al. [20] developed a self-contained, end-to-end system for the translucent resin to produce high-frequency color texture. A. Brunton et al. developed techniques [21, 22] for precise and efficient material placement control in multi-jet 3D printers for halftoning, vital in accurate color reproduction. X. Wei et al. [11, 23] demonstrated that the response surface methodology (RSM) and multilayer perceptron (MLP) neural network model perform well in predicting the measured color. These studies, however, were carried out on standard XYZ build platforms, with industrial Stratasys J750 PolyJet or HP Multi Jet Fusion (MJF) printers as the primary printers.

Studies [24, 25] have shown the significant influence of build orientation, i.e., planar, vertical, and inclined surfaces, on the surface quality and roughness of MJT parts. G. Kim and Y. Oh [26] reported that the surface quality of MJT printing is superior to SLA printing on all inclined surfaces except for the vertical surface, which has an inclination of 90°. Build orientation can also affect the surface appearance of 3D-printed parts. Manufactured objects can also be designed so that they appear differently from various viewpoints or by using the reflection properties of colors to achieve viewpoint-dependent appearances [27]. A few studies have mentioned the rotary build platform model of MJT technology [27, 28] and the liquid jetting at a rotary disk [29]. However, the effect of centrifugal force caused by the rotating build platform on shaping the layers and color quality has yet to be investigated.

Using rotational 3D printing, 3D printers may become smaller and easier for office applications. Different patterns are created on the surface because the tray rotates about a vertical axis, presenting new challenges. Therefore, it will be necessary to examine the surface texture and the quality of 3D-printed objects to develop rotational 3D printing methods. Accordingly, this work presents a texture study to statistically analyze connections between observed color and four PolyJet control parameters, including the specified color, design thickness (Δt), swath (manufacturing track) location on the build platform, and finish type. In order to clarify the contribution of the rotary tray to the color appearance of the samples, we studied the texture and layers of the samples manufactured at different places on the build platform. At the end of this work, we examined the possible conditions of color reproduction using a PolyJet 3D printer by evaluating multivariate analysis over the studied parameters and response variables.

2 Materials and methods

2.1 Experimental design

The role of printing location on the build platform (swath), the thickness of layers, color, and finish type is studied using a full factorial design of experiments as three control factors connected to the measured color. The Stratasys J55 3D printer was used to prepare the samples. A J55 placement zone consists of three areas of the same width: inner, mid, and outer (Fig. 1). The innermost location of the parts should be utilized first for optimal placement and reduced build time. The finish types between the colored layer and white bottom substrate were selected glossy on glossy (GoG) and glossy on matte (GoM) for studying as-printed samples. The specimen dimensions were $10 \times 10 \times 3.5$ mm^3 for color study (Fig. 2) and $60 \times 13 \times 3.5$ mm^3 for texture evaluation and trial color evaluation, respectively. The thresholds for each parameter were chosen to eliminate the influence of post-processing, as well as the limitations imposed by processing software and the 3D printer. For instance, the matte surface finish was avoided due to surface alteration during the support removal process. Furthermore, parts were designed with the minimum size required for measurement to counteract the effect of extended radial layers.

Fig. 2 As-printed MJT samples for color evaluations as observed under D50 daylight illumination

The primary specimens were 3 mm thick with 1.5-mm support material at the bottom, 1-mm white background, and 1-mm colored material on top (Fig. 2). This design method is based on Stratasys best practices for PolyJet and according

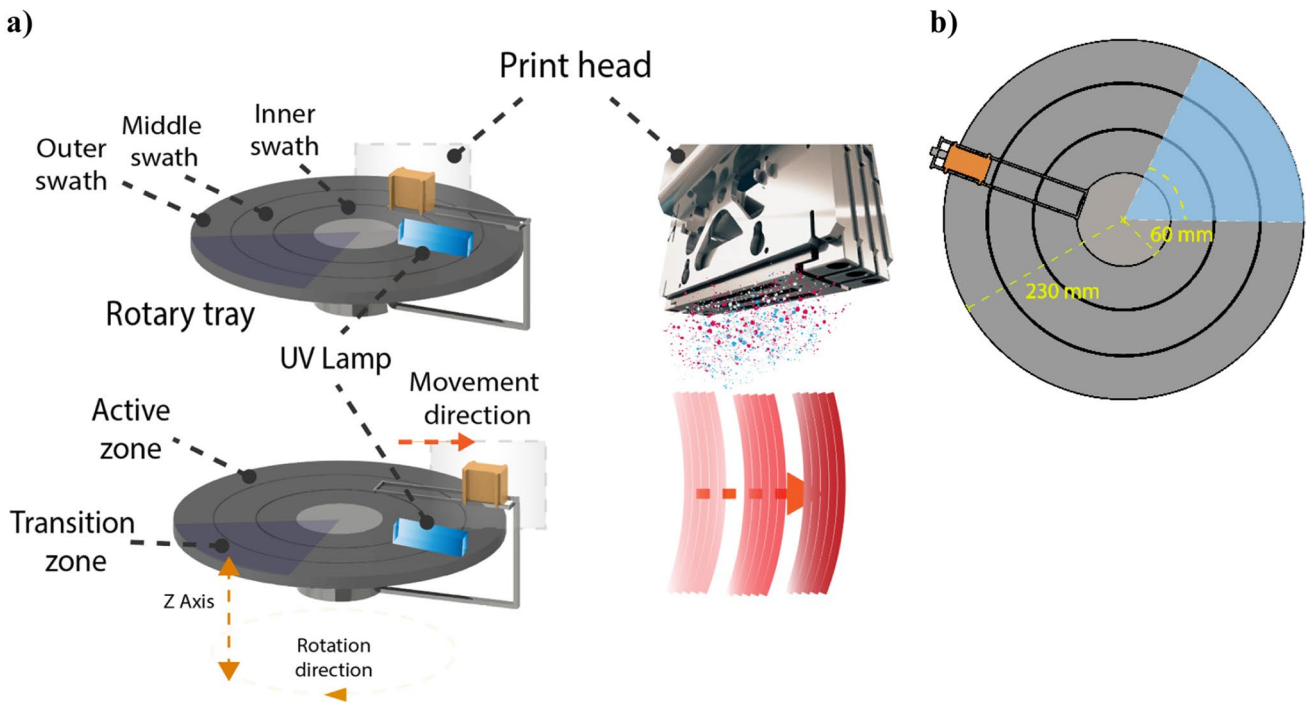

Fig. 1 **a** Illustration of swathes and main zones of the rotary tray. **b** Top view of the swathes with the same width (60 mm) in a J55 PolyJet 3D printer. Samples were printed in a swath from the inner zone toward the outer area of the tray

to Pantone validated color matching system. It states that printed parts should have a wall thickness of at least 1-mm white background for optimal color reproduction. Since the defects and errors in observed CIEL*a*b* values for replicated samples were minimal in the trial experiments, one piece is studied under each experimental condition for the main investigation. In order to investigate the influence of each printing process parameter on the color quality, two sets of experiments have been conducted to reach the optimum condition using the minimum required samples. Levels for each of the experiments are shown in Table 1. In experiment 1, samples with a thickness of 1 mm in the colored layer were manufactured in different swaths. As part of experiment 2, samples with different thicknesses were 3D-printed in the middle swath of the rotating disk of the 3D printer. In both experiments, two different surface finishing options were selected between the white background and CMYK-colored layers. A total of 48 color samples were subjected to in-depth spectral analysis.

2.2 Measurements

A Konica Minolta CS-2000 tele-spectroradiometer (TSR) was used to determine the spectral radiance at the 3D-printed object surface in the 380–780 nm spectral range (Fig. 3). The physical sampling interval was 10 nm, whereas the optical resolution was 1 nm. Using 45:0° viewing geometry, the surface of the 3D-printed item was evaluated according to CIE Publication 15.2 [30]. Each series of measurements was calibrated with the white Spectralon patch (Barium sulfate coating). The obtained radiances have been averaged from measurements in the field of view of 0.2° on three-centric regions of the surfaces to overcome edge loss in measuring reflectance on semi-translucent materials. At least ten horizontally distrusted 3D-printed layers were present at each targeted location on the studied surface. Any site having odd coloration, external particles, or support materials was avoided.

Measurements were taken in a dark room to avoid errors caused by other light sources such as ambient lighting. Radiance spectra have been recorded considering noise reduction due to the possible stray lights in the darkroom of the measurement.

Calculations were performed using the computational color science toolbox in MATLAB 2021 [31]. For this purpose, CIEXYZ tristimulus values were calculated according to the CIE 2° color-matching functions, using the sample reflectance and under the D50 illuminant. CIEL*a*b*

Table 1 Experiments and their levels

Color	Finishing	Experiment 1		Experiment 2	
		Swath	Thickness (mm)	Swath	Thickness (mm)
Cyan	GoG and GoM[a]	Inn, mid, and out[b]	1	Mid	0.2, 0.5, 1, and 2
Magenta	GoG and GoM	Inn, mid, and out	1	Mid	0.2, 0.5, 1, and 2
Yellow	GoG and GoM	Inn, mid, and out	1	Mid	0.2, 0.5, 1, and 2
Black	GoG and GoM	Inn, mid, and out	1	Mid	0.2, 0.5, 1, and 2

[a]GoG, glossy on glossy finish; GoM, glossy on matte finish

[b]Inn, inner (r-tray < 120 mm); Mid, middle (120 mm < r-tray < 180 mm); O, outer (180 mm < r-tray < 230 mm) swath

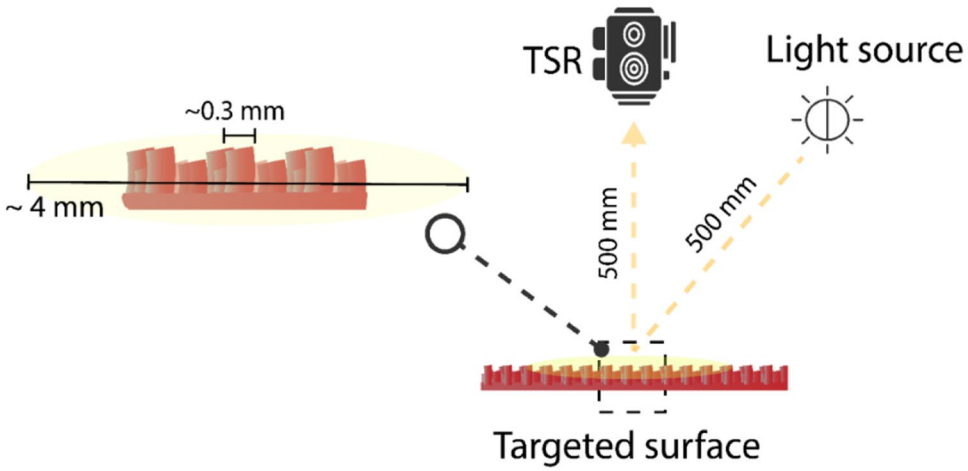

Fig. 3 Schematic diagram of the measurement setup using a tele-spectroradiometer. The enlarged area represents the comparable size of the measurement area and the average width of the uppermost layers

coordinates were further calculated according to CIE1976 [30] and using the CIEXYZ tristimulus values in Eqs. 1–3.

$$L^* = 116\left(Y/Y_n\right)^{1/3} - 16 \tag{1}$$

$$a^* = 500\left[\left(X/X_n\right)^{1/3} - \left(Y/Y_n\right)^{1/3}\right] \tag{2}$$

$$b^* = 200\left[\left(Y/Y_n\right)^{1/3} - \left(Z/Z_n\right)^{1/3}\right] \tag{3}$$

where X_n, Y_n, and Z_n are the tristimulus values of a specified white achromatic stimulus (Spectralon).

CIEDE2000 [32] colorimetric differences as given in Eq. 4 was calculated between the object printed on the three swaths. CIEL*a*b* values obtained from the objects with 1-mm thickness printed in the middle swath were used as reference measurements when calculating the CIEDE2000 difference.

$$\text{CIEDE2000} = \sqrt{\left(\frac{\Delta L^*}{k_L S_L}\right)^2 + \left(\frac{\Delta C^*}{k_C S_C}\right)^2 + \left(\frac{\Delta h^*}{k_h S_h}\right)^2 + R_T f(\Delta C^* \Delta h^*)} \tag{4}$$

In Eq. 4, L*, C*, and h* refer to lightness, chroma (the distance out from the neutral axis—saturation), and hue as defined in CIE15.2 [30]. The constant values of k_L (lightness), k_C (chroma), and k_h (hue) are usually unity [33]. Other parameters refer to the hue rotation term (R_T) and the compensation for lightness (S_L), chroma (S_C), and hue (S_h).

A total of nine printer objects, including three pieces printed on each swath, have been scanned vertically and horizontally using a coordinate measuring machine (CMM) model Zeiss DuraMax. The step width was set at 10 µm, a probe radius of 1.5 mm was chosen, and the machine was accurate to 2.4 µm. A desktop 3D scanner (Autoscan Inspec, Shining 3D) was utilized in dark conditions. An 8-times rotation was made with the specimens mounted on a turntable every 45° until a 360° view was achieved. An object was scanned with an accuracy of ≤ 10 µm under a blue-light projector emitting structured-light patterns. The distorted dimensions are measured using two 5.0MP CCD cameras on the scanner. The registered point cloud is collected from multiple scans at various object orientations. All digitization was merged using UltraScan 2022 software, and a raw texture-based model in STL (stereolithography) format was created in MeshLab (v2022.02). The 3D coordinates of the object were compared with the CMM results. Following the CMM acquisition, the raw data was processed in Gwyddion (v2.59) to determine layer thickness and heights as well as the topography.

Holmberg et al. [34] examined the surface microstructure changes during machining processes based on the full width at half maximum (FWHM) analysis and optical microscopy study. We utilized the FWHM values to analyze the height distribution. Texture evaluation allows reconstructing of the profile of additive manufacturing and realizing data registration and appearance evaluation.

Surface features in AM technology are the presence of microscale repetitive layers in the surface texture of 3D-printed objects [35]. There are two approaches to the analysis of texture: structural (analytical), where primitives are analyzed, and syntactical (statistical), where statistics are used to determine the texture of the entire textural region [36]. Autocorrelation and Fourier analysis are the most common structural methods for the analysis of texture, while for statistical analysis, co-occurrence matrices or run-lengths are common methods. To evaluate the surface texture analytically, we used Fourier analysis.

The FFT (fast Fourier transform) method removes all high-frequency noise, revealing the actual signal [37]. Several authors have demonstrated that the power spectral density (PSD) of a contact area determines the morphology of its surface [38–40]. Accordingly, we developed an algorithm for evaluating the 3-D geometry of additive manufacturing surfaces. Our method transforms 3D texture into a 2D coarseness profile using 1D Gaussian filtering and FFT filter smoothing. The asymmetric profiles associated with shape have been subtracted from the repeated texture profiles using polynomial fitting tools in OriginPro v9.5 to remove the effects of the form on the texture results.

According to ISO 16610–31, the robust regression Gaussian filter calculates weights individually for a primary profile and a waviness profile using iterative algorithms. Using this filter, the mean line is strongly associated with the general trend of the surface profile with spike discontinuities such as deep valleys and high peaks and is unaffected by outliers. The FFT algorithm was implemented to remove high-frequency noises and reduce the waveforms to the absolute magnitude and phase data in a frequency domain. The power output versus frequency spectrum of the surface profiles was examined by FFT spectra of signals, where power is normalized as the space (time in standard notations)-integral squared amplitude (TISA) using the following equations:

$$P_{xx}\left(e^{j\omega}\right) = \sum_{m=-\infty}^{\infty} r_{xx}(m)e^{-j\omega m} \tag{5}$$

$$\text{TISA(Power)} = \frac{\Delta t\left(R_e^2 + I_m^2\right)}{n} \tag{6}$$

where $P_{xx}\left(e^{j\omega}\right)$ is the power density or spectrum (PSD), $r_{xx}(m)$ is the auto-correlation function of the input signal, Δt is the sampling interval, R_e and I_m are the real and imaginary parts of the transform data, and n is the length of the input sequence. In order to mitigate leakage, the single rectangle window function is applied as follows:

$$N/\sum_{n=0}^{N-1} w(n)^2 \tag{7}$$

where $w(n) = 1$ for $0 \le n \le N-1$, and zero otherwise.

The statistical procedures were based on ISO/TS 23,031:2020 (E). Accordingly, it is possible to evaluate the color difference between reference and test spectra and the root-mean-square error between them using the root-mean-square error (RMSE) and the mean color difference from the mean (MCDM) [41]. The following are the definitions:

$$\mathrm{RMSE} = \sqrt{\frac{1}{N}\sum_{i=1}^{N}(r_{r,i} - r_{t,i})^2} \tag{8}$$

$$\mathrm{MCDM} = \frac{1}{N}\sum_{i=1}^{N}\Delta E(C_i, C_m) \tag{9}$$

where r_r and r_t are the references and test spectrum, N is the number of reflectance readings, and C_i and C_m are the coordinate colors of the ith measurements and the average reflectance of all measurements, respectively. The RMSE of each quantitative variable is obtained to perform the spectral analysis, comparing the spectra of the target surfaces.

Multivariate analysis of the studied parameters and the response variables were run using principal component analysis (PCA) and the listwise Spearman rank correlation coefficient (Spearman rho, also signified by rs) due to small sample sizes [42]. PCA is a robust way of reducing the dimensionality of data. The raw data is linearly transformed into a set of principal components, which show the most significant variations in the raw sensor data. The PCA method of estimating correlations is a multivariate extension of linear regression to matrices containing independent and dependent variables [43, 44]. Two sets of variables can be viewed as asymmetrical, as one batch is considered an independent variable such as printing parameters, and the other as a dependent variable. In this work, the matrix of appearance variables included measurements of color attributes including dL, dC, and dh.

Furthermore, Spearman rho was utilized to measure the relationship between the frequency of print variables and color attributes. It is a non-parametric measure for categorical data, which evaluates monotonic relationships of data that are not normally distributed regardless of linearity. Spearman rho of + 1 or − 1 refers to the case where each variable is a mathematically ideal monotone function of the other [42]. Statistical analyses were carried out using OriginPro v9.5.

3 Results and discussions

3.1 Texture evaluation

An optical image of a studied specimen and the corresponding STL model generated by the 3D scanner is shown in Fig. 4; a semicircle pattern can be observed in the corresponding surface texture image for the 3D-printed layers (Fig. 4c).

Using CMM data, Fig. 5 illustrates a closer look at additively manufactured layers and the results of an FFT examination applied to height maps (Z height). The strong peaks for averaged results in Fig. 5c confirm the periodic nature of the layers and the associated surface texture in the specimens studied. Arithmetic means of the periodic distance between layers can be obtained by calculating the average frequency of distances for the PSD peaks.

According to Fig. 5b, the obtained MJT surfaces were relatively smooth with a Z height of less than 15 µm. In addition, height distributions followed a normal distribution. There is a lack of understanding as to the mechanism by which texture affects color appearance on smooth surfaces in semi-translucent MJT materials. It has been suggested

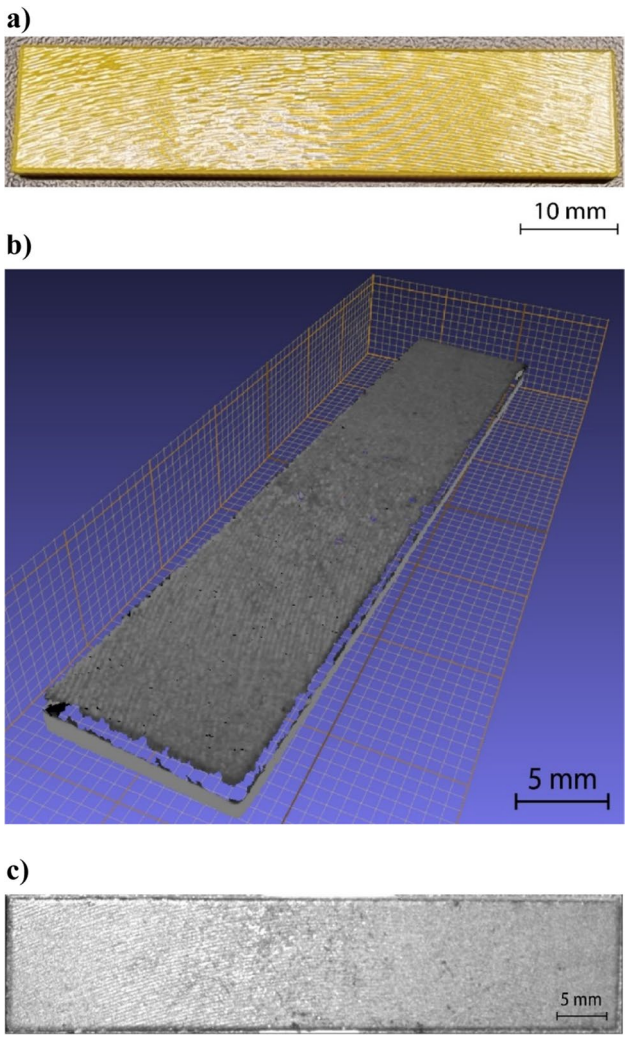

Fig. 4 **a** 3D-printed samples for texture evaluation, **b** STL model generated from 3D scanning, **c** 2D texture-based model created from the point cloud

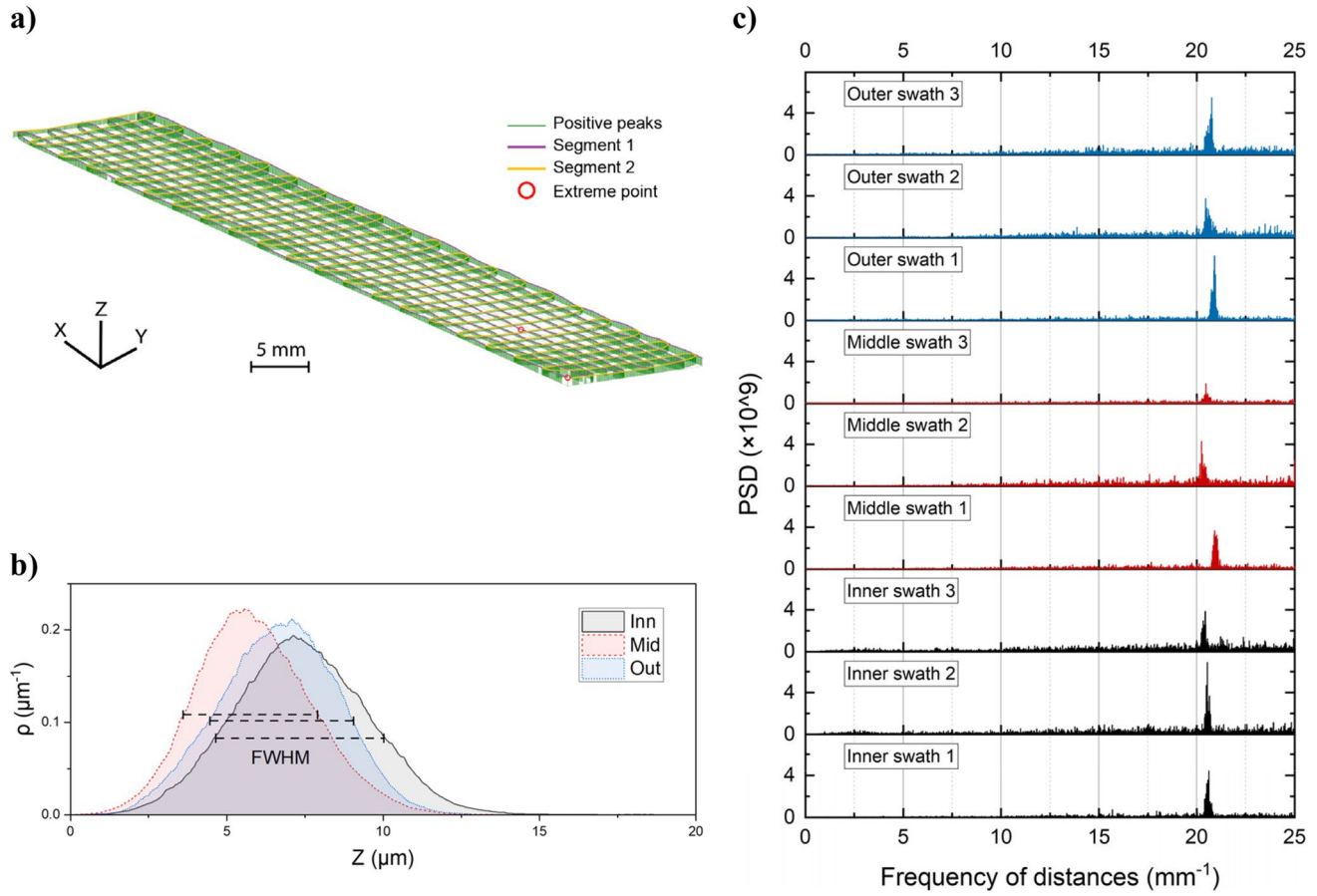

Fig. 5 **a** Contour plot showing the scanning strategy (exaggerated *Z* profile), **b** Profile of *Z* height distribution, and **c** power spectral density (PSD) results along with the scanning profile

that the texture of the surface influences how light is scattered and how the color is measured as a result [45]. J. H. Bae et al. [46] reported as the visual texture rank increased, inkjet-printed samples were perceived as darker. Nevertheless, this effect was not consistent across colors. Accordingly, the texture of a surface can affect chromatic induction, which is essential for color constancy under full-field viewing conditions.

Table 2 lists the arithmetic mean height of asperities over vertical and horizontal scanning directions according to Fig. 5. CMM measurements show that the mean layer height and FWHM for separate locations on the build platform exhibit a meaningful correlation, where the minimum arithmetic means of layer height (5.69 μm) and FWHM (3.84 μm) belong to the middle swath. Table 2 also suggests that layers become increasingly thinner from 305 to 303 μm as the selected tray radius increases. The difference can be explained by the higher centrifugal force on the build platform in the outer area of the disk. By moving from the inner swath to the outer edge of the tray, the print head of a 3D printer may create a closer layer compared to previous layers.

3.2 Color measurement

The chromaticity diagrams in Fig. 6 represent the map of color space for the average of u′ and v′ values corresponding

Table 2 Mean height of asperities over vertical scanning direction

Swath	Mean layer distances (μm)	RMSE (μm)	Mean layer heights (μm)	RMSE (μm)	Mean FWHM (μm)	RMSE (μm)
Inner	305.96	1.12	7.45	0.56	4.79	0.16
Middle	305.78	4.14	5.69	0.86	3.84	0.33
Outer	303.33	2.75	7.14	0.36	4.48	0.01

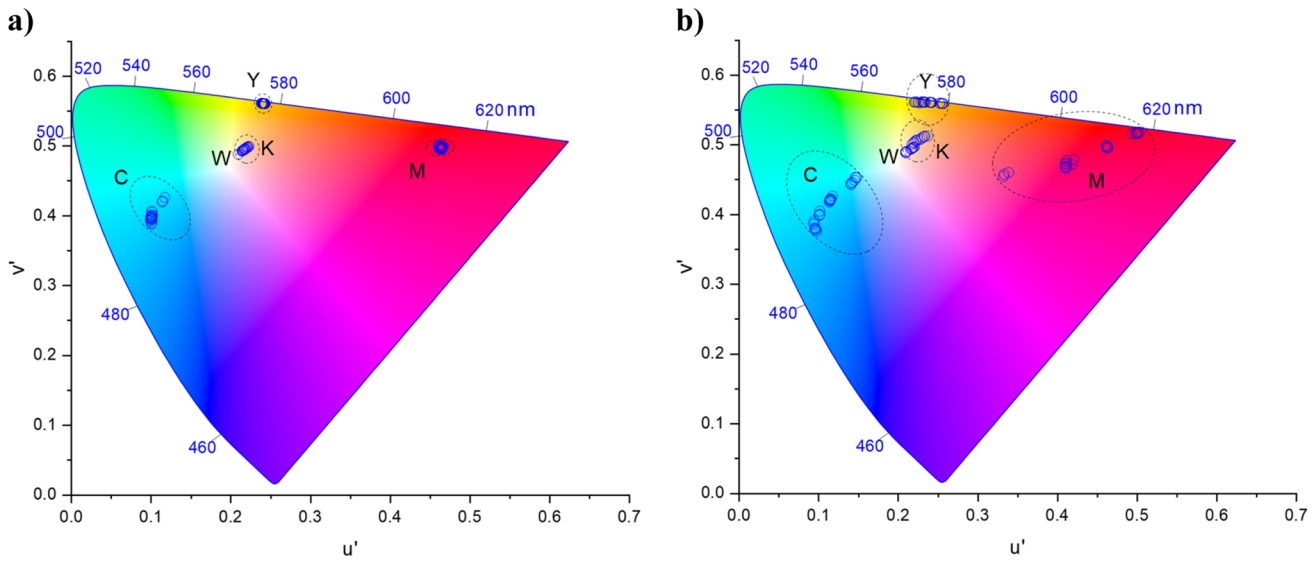

Fig. 6 Hue stimuli in the CIE1976 u', v' chromaticity diagram for specimens manufactured at different **a** swathes and **b** thicknesses. The wavelengths between 420 and 680 nm are indicated in blue on the graph. C, cyan; M, magenta; Y, yellow; K, black; W, D50 white reference

to each specimen. CMYK points were closer on surfaces printed with different swathes than on objects with various thicknesses. It basically implies a higher color difference because of the thickness variation compared to swathes.

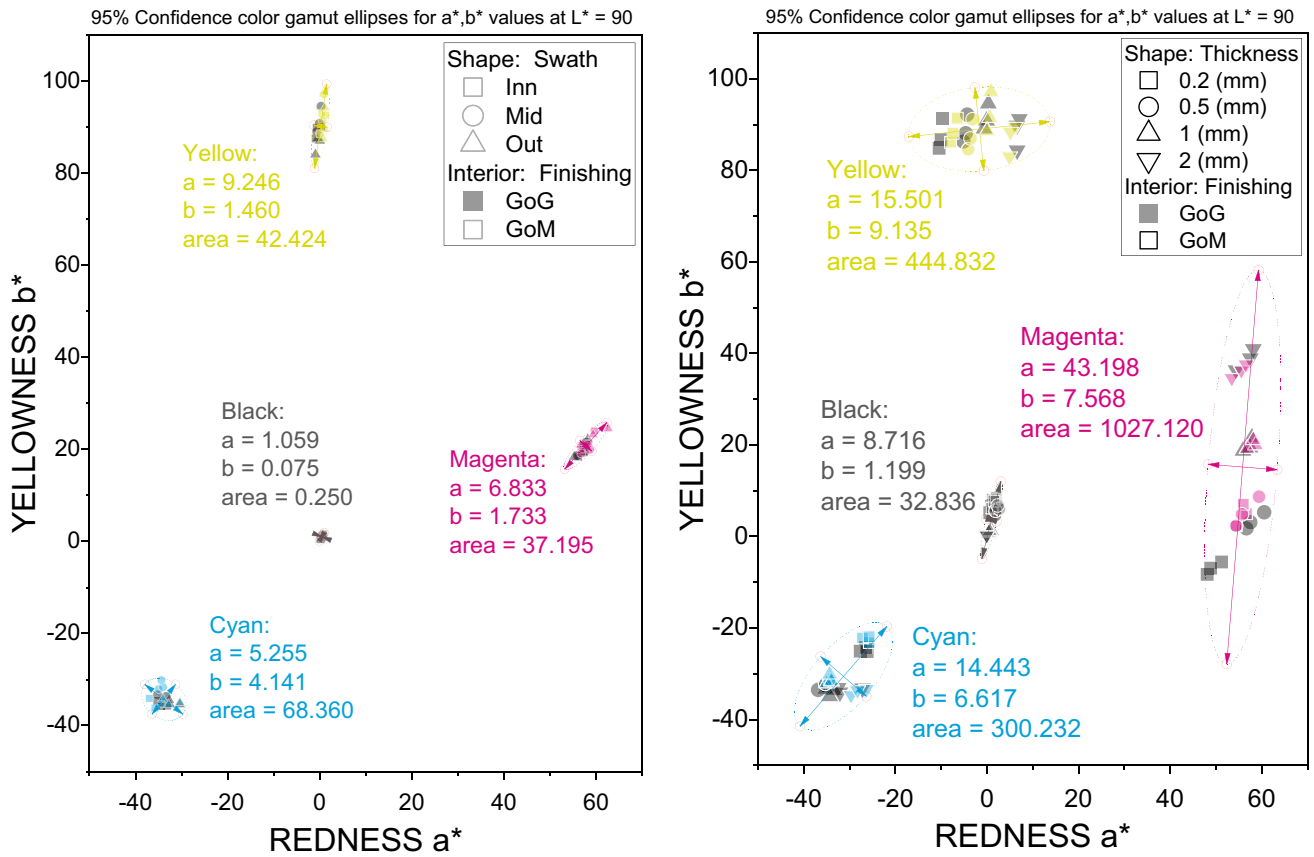

Fig. 7 95% confidence color gamut ellipses and yellowness versus redness for specimens related to **a** swath and **b** thickness experiments

The values of redness (a*) and yellowness (b*) at the same lightness (L*) also confirmed the same trend in the CIEL*a*b* color space. In Fig. 7, the 95% confidence color gamut ellipses suggest that magenta was significantly more sensitive to thickness than swath selection. Furthermore, thicker yellow and magenta objects resulted in greater b* and a* values, while the opposite held true for black and cyan objects. The color was more stable in the same lightness among the black samples despite varying printing conditions. For these samples, finishing played no significant role.

The spectral properties of surfaces and illumination also play an essential role in determining color. As a result, when evaluating color quality, it is necessary to consider both colorimetric and spectral measurements [47]. Figure 8 depicts how cyan and yellow colors shifted to lower spectral values for outer swathes than inner areas. In contrast, magenta exhibited the opposite behavior, and black samples were almost immune to spectral shift. On the other hand, lower thicknesses of the CMYK layers (Fig. 9) resulted in higher spectral reflectance for all samples, which indicated that the increased thickness accounted for the lightness reduction and lower spectral reflectance regardless of surface color.

In general, more significant MCDM color differences were observed for the thickness experiment compared to the swath study (Fig. 10), as observed from chromaticity diagrams in Fig. 6. All colors studied, except black, showed the lowest CIEDE2000 values when the middle swath was selected compared to the inner area. CIEDE2000 between central and outer,

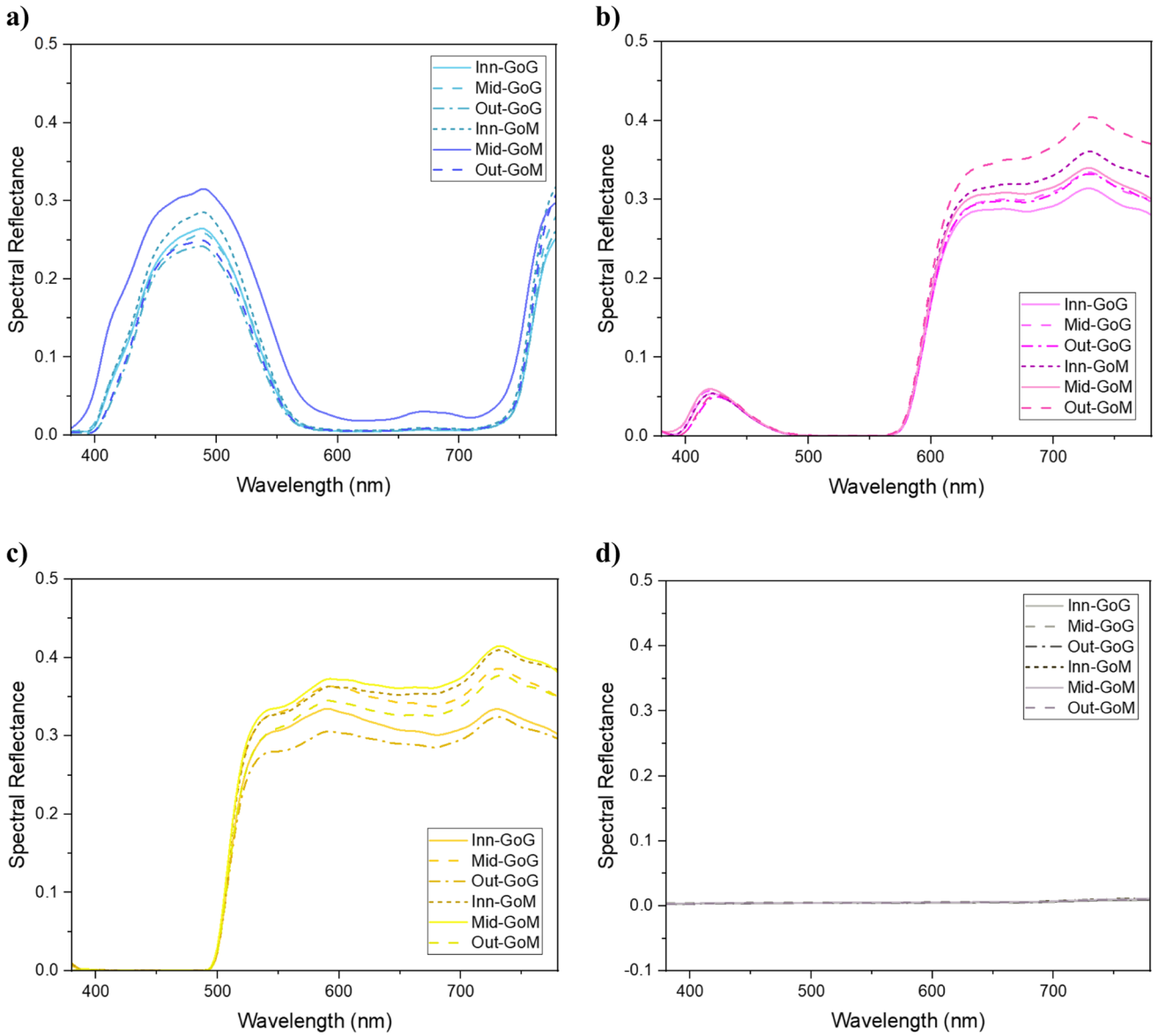

Fig. 8 Reflectance of **a** cyan, **b** magenta, **c** yellow, and **d** black specimens 3D-printed at different swathes on the build platform

however, produced a different response. Higher layer heights may be compromised by the closer layer distances in the external zones of the tray. According to Table 2, this result aligns with the texture measurements and higher lightness variation due to higher layer heights. It allows parameterization of the swath selection to produce the lowest color differences in the middle swath compared to the other areas of the build platform (Fig. 10a). The transfer distance for light over the 3D-printed structures might be decreased due to a more evenly distributed texture with lower layer heights for this swath.

According to CIEDE2000 for color matching in paper-based printing [48, 49], a color difference of 1 is barely perceptible to the average human. An experienced observer notices CIDE2000 between 1 and 2. Color difference from 2 to 3.5 is also noticeable to an inexperienced observer. However, 5 < CIDE2000 is not an acceptable match for commercial printing presses. The calculated color differences in Fig. 10a and b indicate that CIDE2000 ranges were less than 5. Yellow samples and surfaces with the GoM finish of cyan parts had the most significant color difference visible to inexperienced observers. The appearance difference between black and magenta colors was challenging to distinguish due to their color. Considering commercial purposes, all results were acceptable when switching between segments on the tray. Since human vision is more sensitive to color differences when two colors touch [50], mixing CMYK colors may result in noticeable color differences.

As for the variations in the thickness of colored layers, on the other hand, rather than yellow at the lower thickness and black at the higher thickness, the rest were in assorted

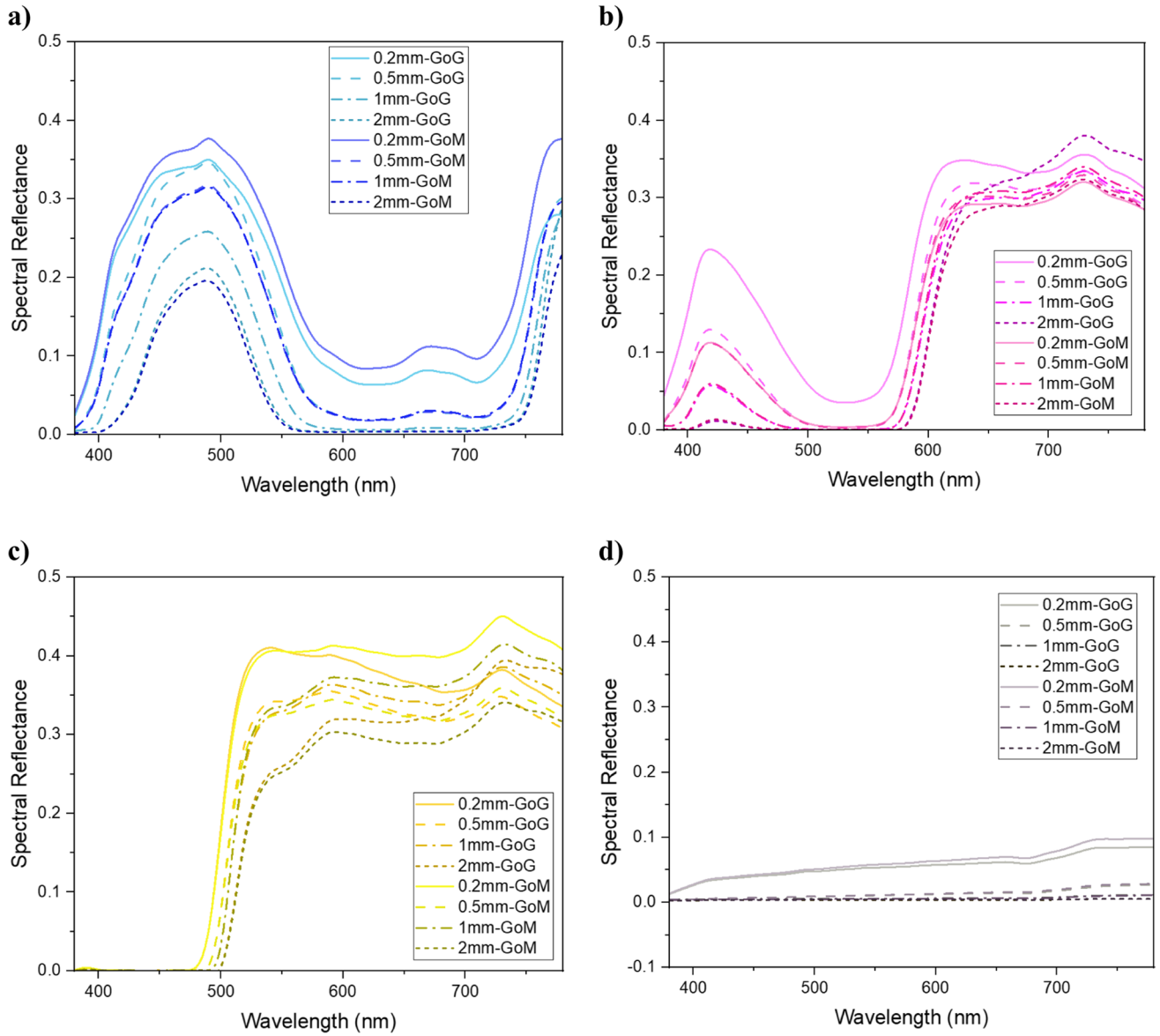

Fig. 9 Reflectance spectra of **a** cyan, **b** magenta, **c** yellow, and **d** black specimens 3D-printed at different thicknesses

colors and were not acceptable for commercial color reproduction. Compared to 1-mm thick colors, 0.5-mm thickness resulted in a more negligible color difference than 2- and 0.2-mm thickness (Fig. 10c). Similar to the swath study, the CIEDE2000 values were lower for black-colored surfaces. Choosing the GoM finish for cyan, magenta, and yellow colors increased the color difference in the swath experiment (Fig. 10b). However, it did not contribute considerably to thickness evaluation (Fig. 10d).

Figure 11 signifies the relationship between the two main color attributes affected by swath selection. The Euclidean distances revealed that as the radius of the layers on the substrates increased, the variation in lightness and hue values was not linear. Because the absolute difference in lightness and hue between the inner and outer areas of the build platform was minimal when the difference between the mid and inn and out swaths was considered. Further analysis from Table 2 revealed that texture results were able to differentiate the color attributes affected by layers. Consequently, since the layer height of the middle swath differs the most from other swathes, lightness and chroma are more variable, with a more substantial influence on lightness.

Figure 12 displays the MCDM color difference versus RMSE values. In the swath experiment, black was the color with the slightest variation and produced the most consistent results. Cyan had a more pronounced color difference than red and yellow, but a lower RMSE made it less unpredictable to swath changes. Considering thickness changes, both cyan and black color reproduction had

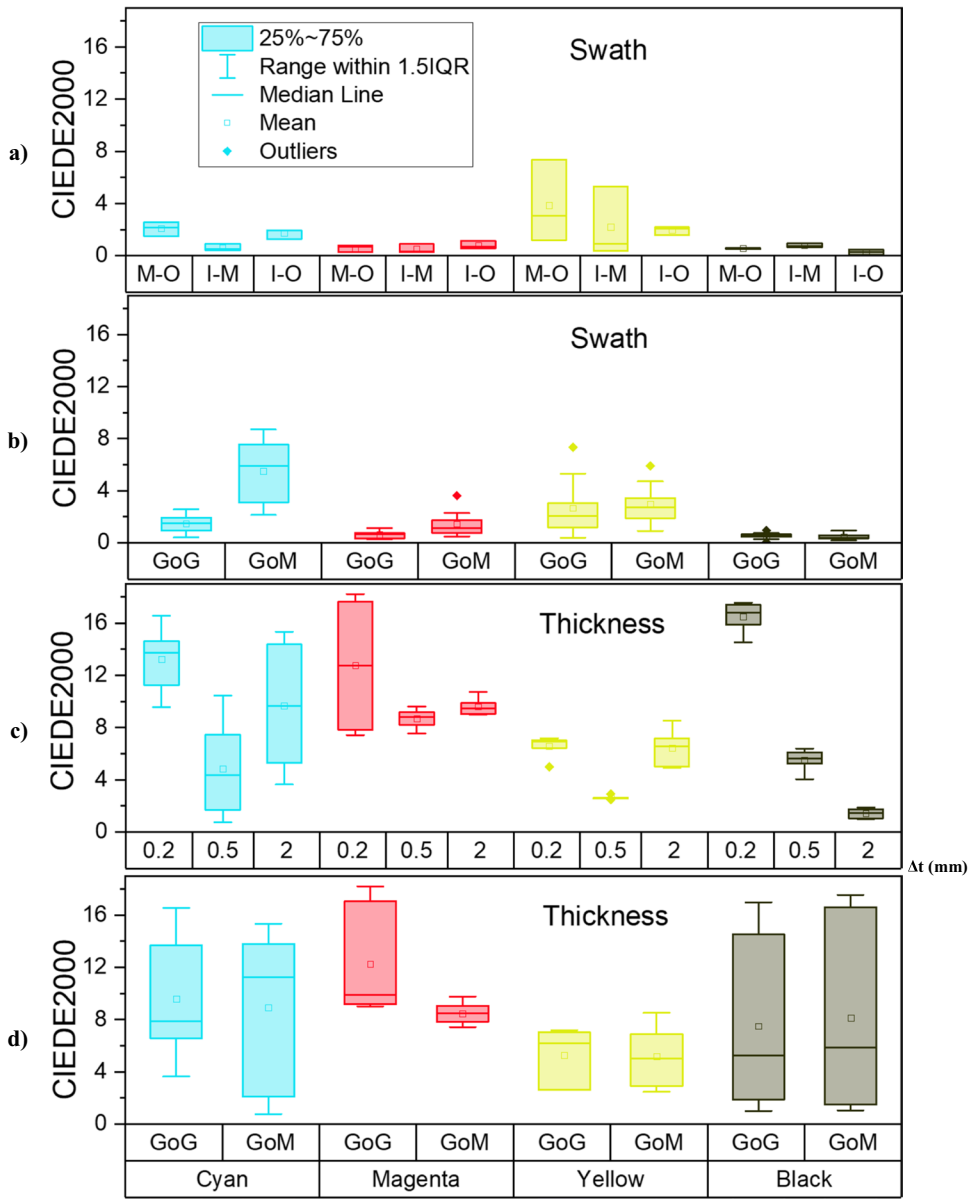

Fig. 10 CIEDE2000 color difference due to manufacturing parameters for swath and thickness experiments. The influence of **a** choosing different swathes using GoG finish, **b** finishing condition for different swathes, **c** F*t*, and **d** finishing condition for different thicknesses on CIEDE2000. Δ*t*, color layer thickness compared to 1 mm recommended by the manufacturer of the 3D printer; IQR, interquartile; I-M, inner swath versus middle swath; I-O, inner swath versus outer swath; M–O, middle swath versus outer swath

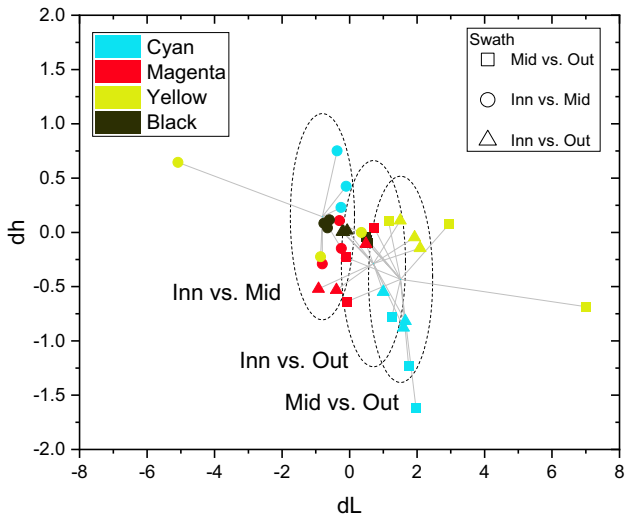

Fig. 11 The Euclidean distances with 0.95 confidence area for the swath experiment

significantly higher MCDM and RMSE. The reproducibility of yellow appeared to be more sensitive to swath selection than thickness variation. However, color differences for all CMYK colors were nearly double due to colored layer thickness differences.

3.3 Multivariate statistical analysis

The PCA correlation type results were presented as ranking diagrams, which used figurative symbols. The direction of maximum change is indicated by arrows on print variables and color attributes. A high correlation is observed between the variables when placed in close or the same direction, and low correlations when placed in the opposite direction. The two lines at a 90°-angle indicate no correlation between the variables. Table 3 implies that the cumulative inertia for the first and the second principal components (PC1 and PC2) reached 91.03% for swath and 83.13% for thickness experiments. Moreover, PC1 and PC2 represented eigenvalues greater than 1. Therefore, based on the Kaiser criterion, two PCs would be appropriate enough to explain the correlation among data in PCA.

The loading plots (Fig. 13) demonstrate lightness had a robust positive effect on PC1 and almost neutral on PC2 for swath evaluation. In contrast, hue had a meaningful negative impact on PC1 and a considerable positive impact on PC2. In contrast, both lightness and hue acted reversely for PC1 and PC2 concerning the variation in thickness. Chroma

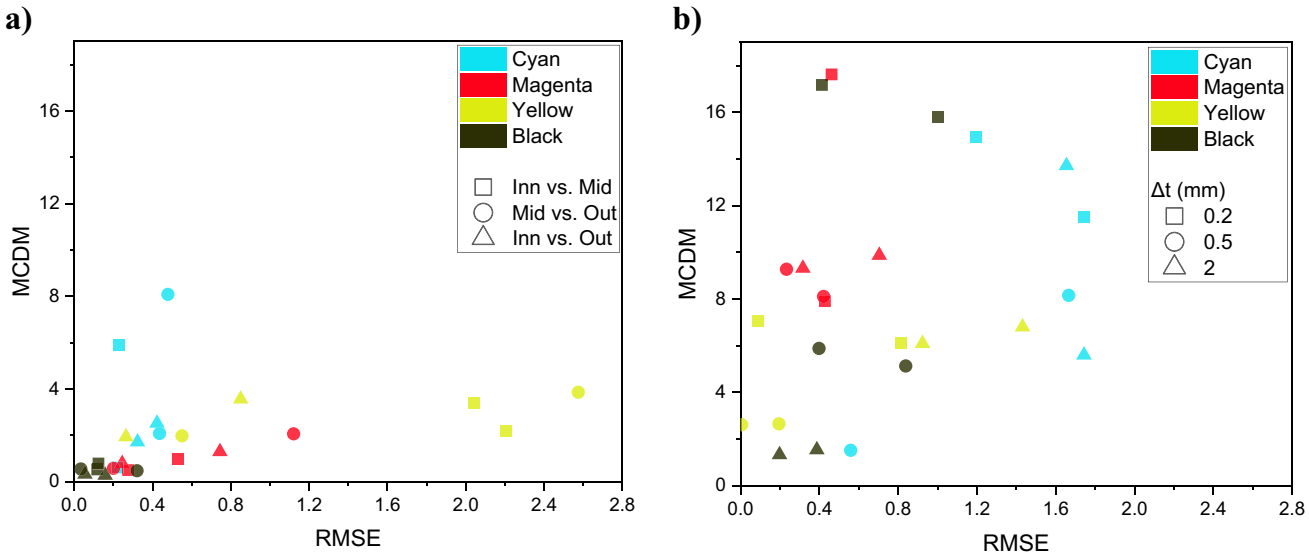

Fig. 12 RMSE versus MCDM for **a** swath and **b** thickness experiments

Table 3 Principal components ranking according to their cumulative roles in PCA

PC ranking	Experiment 1: swath			Experiment 2: thickness		
	Eigenvalue	Percentage of variance (%)	Cumulative (%)	Eigenvalue	Percentage of variance (%)	Cumulative (%)
1	1.67	55.82	55.82	1.36	45.41	45.41
2	1.05	35.21	91.03	1.13	37.72	83.13
3	0.26	8.96	100	0.50	16.86	100

positively influenced both PC1 and PC2 in both experiments. Accordingly, variations in the printing parameters have affected variations in tristimulus color attributes.

Spearman correlation coefficient was used to establish the significance of each manufacturing condition (Fig. 14). A correlation coefficient greater than 0.50 and 0.70 is considered moderate and robust correlations, respectively if P values are less than 0.05. P values less than 0.01 and Spearman rho higher than 0.60 are generally valid co-occurrences [43]. Accordingly, the correlation coefficient with rs = 0.87 between thickness alteration and dL is strong (P < 0.001). Based on the rank correlation, swath and thickness selection had a more considerable effect on lightness and chroma than color, and the influence of finishing between colored and white layers was negligible. While dL had the greatest impact on color appearance, the effect varied depending on the ink materials specified. Following texture evaluation, results indicate that the variation in swath and thickness, influencing the surface texture and geometries, significantly alters the appearance of color due to the lightness alteration.

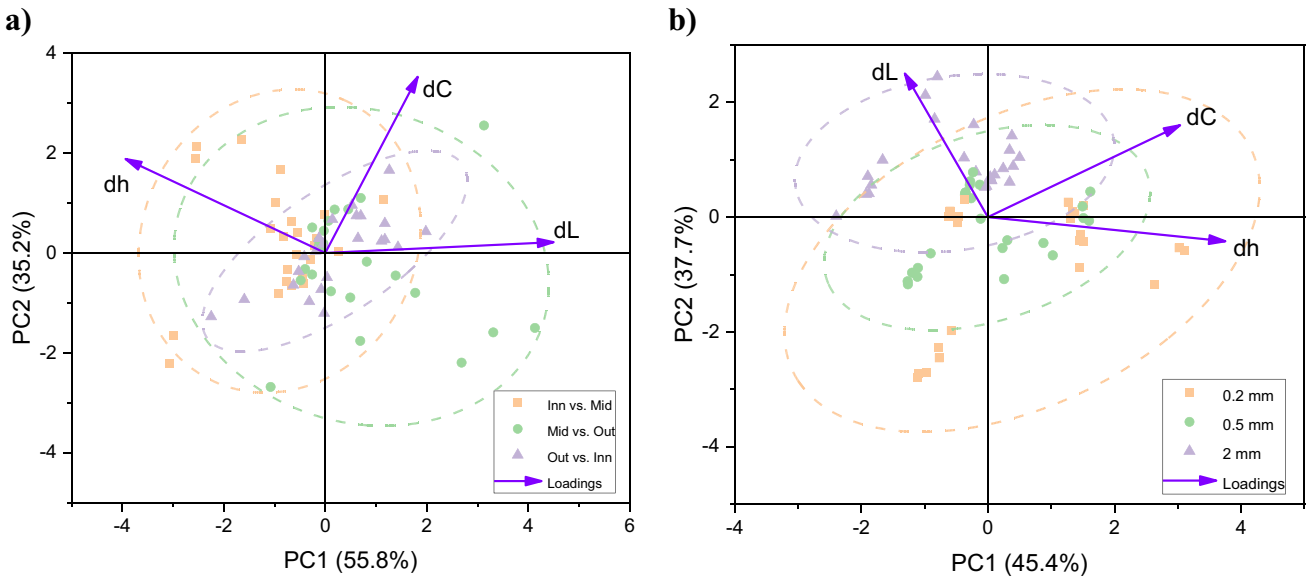

Fig. 13 Principal components analysis (PCA) ordination diagram (biplot) for **a** swath and **b** thickness experiments. Denoted points show sample scores, 95% confidence ellipses show for the same-colored points, and loading vectors represent explanatory variables (3D printing parameters) and response variables (color attributes), respectively. Horizontal and vertical axes denote the first and second principal components (PC1 and PC2). Correlations between variables are represented by angles between vectors, where the smaller the angle, the greater the correlation. Vectors pointing in the same direction represent positively correlated variables, and vice versa

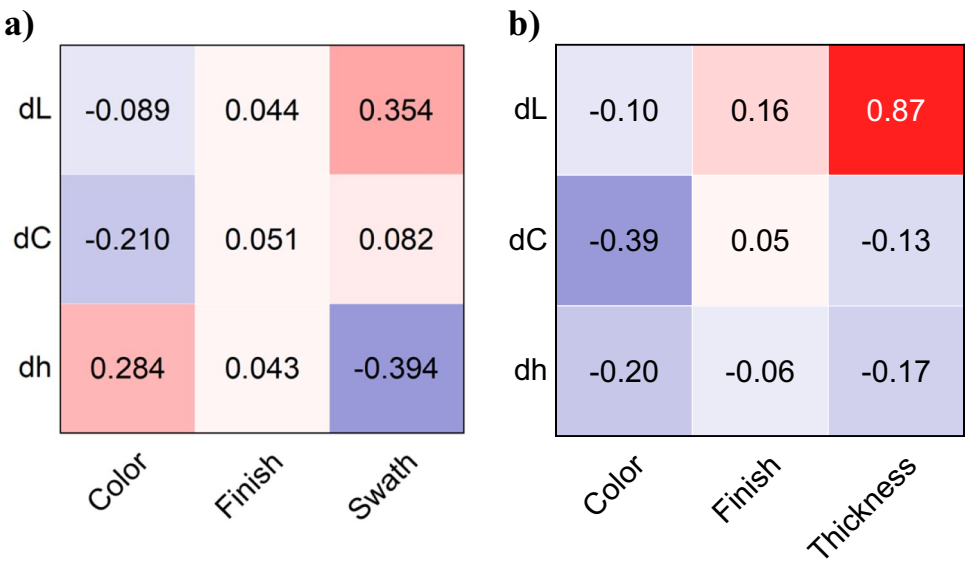

Fig. 14 The Spearman correlation coefficient results for **a** swath and **b** thickness experiments

4 Conclusions

This study investigated relationships between observed color and four PolyJet control parameters: specified color, design thickness, swath location on the build platform, and finish type between colored and substrate layers. We studied the texture and surface layers of samples 3D-printed at separate places on the build platform to determine the effect of the rotary tray on color. Triplets of chromaticity coordinates or standard color values are used to indicate the color of a particular object. The following conclusions were drawn from this study:

The CMM measurement showed that manufacturing in the middle zones resulted in more low-height asperities. Based on the obtained power spectral density (PSD) versus the frequency of distances, the surface asperities could be assumed to be periodic. Therefore, the height distribution was representative of the heights of repeated layers. These results were observed by scanned 3D models of the surface. As a result, the surface layers in the middle of the rotary build platform were thinner.

PCA and listwise correlation analysis correlated the influence of lightness on the higher color difference for thickness experiments. We used multivariate analysis to determine the optimal conditions for color reproduction using a PolyJet 3D printer. While the influence of finishing between colored and white layers was negligible, alteration of swath or thickness, which influenced surface texture and physical geometry, greatly influenced variation in lightness and hue. The color appearance was more sensitive to thickness than swath selection in this regard, which was directly affected by lightness. This, however, was contingent on the ink materials specified. In the swath experiment, the yellow color and glossy colored layer printed on matte white substrate finishing led to a greater color difference. Nevertheless, it was less sensitive to thickness variation than cyan, magenta, and black materials.

Both experiments indicate the importance of adjusting the location on the build platform and thickness during pre-processing. Shorter radial printing generally yields less expensive and faster 3D printing. However, it does not necessarily result in more accurate color reproduction. Printing on different zones of a rotary build platform may also affect the surface roughness, gloss, and translucency. The switching of swathes did not fail samples for industrial color matching. Still, a thickness variation of as small as 0.5 mm could cause most specimens to go above 5 on the CIEDE2000 scale, which resulted in an unnatural appearance due to variation in color reproduction.

Based on the selected 3D printing parameters, color differences could be discernible by an inexperienced observer for the majority of samples. However, color reproduction utilizing rotary disks in PolyJet printers can meet the criterion of color quality in everyday contexts with various illuminations. Combined with our findings, results indicated that the MJT objects had all the relevant visual characteristics, including color, gloss, translucency, shape, shading, and texture, that stimulate the visual representation sufficiently to induce a color difference. As a result, other appearance attributes also should be considered when evaluating the total appearance of parts manufactured by rotational material jetting.

Author contribution All authors contributed to the study's conception and design. Material preparation, data collection, and analysis were performed by Ali Payami Golhin. The first draft of the manuscript was written by Ali Payami Golhin, and all authors commented on previous versions of the manuscript. All authors read and approved the final manuscript.

Funding Open access funding provided by NTNU Norwegian University of Science and Technology (incl St. Olavs Hospital - Trondheim University Hospital) The funding received on this project was from the ApPEARS-ITN project funded by the European Union's H2020 research and innovation program under the Marie Skłodowska-Curie grant agreement No. 814158.

Data availability Data are available at Payami Golhin, Ali, Suneel Sole, Aditya, and Strandlie, Are (2022). Datasets for the submitted paper "Color appearance in rotational material jetting" (version 1) [data set]. Zenodo. https://doi.org/10.5281/zenodo.6640295

Code availability Color toolbox is available at MATLAB Central File Exchange, visit https://se.mathworks.com/matlabcentral/fileexchange/40640-computational-color-science-using-matlab-2e. Other codes are custom-made, and they cannot be shared as they are proprietary.

Declarations

Ethics approval Not applicable.

Consent to participate Not applicable.

Consent for publication Consent to publication has been received from all co-authors before the work is submitted.

Conflict of interest The authors declare no competing interests.

References

1. Vidakis N, Petousis M, Michailidis N et al (2022) High-performance medical-grade resin radically reinforced with cellulose nanofibers for 3D printing. J Mech Behav Biomed Mater 134:105408. https://doi.org/10.1016/j.jmbbm.2022.105408
2. Aslani KE, Korlos A, Kechagias JD et al (2020) Impact of process parameters on dimensional accuracy of PolyJet 3D printed parts using grey Taguchi method. MATEC Web of Conferences. EDP Sci. https://doi.org/10.1051/matecconf/202031801015
3. Aslani KE, Vakouftsi F, Kechagias JD et al (2019) Surface roughness optimization of poly-jet 3d printing using grey Taguchi method. International Conference on Control, Artificial Intelligence, Robotics & Optimization (ICCAIRO). https://doi.org/10.1109/ICCAIRO47923.2019.00041
4. Li Y, Linke BS, Voet H et al (2017) Cost, sustainability and surface roughness quality—a comprehensive analysis of products made with personal 3D printers. CIRP J Manuf Sci Technol 16:1–11. https://doi.org/10.1016/j.cirpj.2016.10.001
5. Fountas NA, Kitsakis K, Aslani K-E et al (2021) An experimental investigation of surface roughness in 3D-printed PLA items using design of experiments. Proc Inst Mech Eng J J Eng Tribol 236:1979–1984. https://doi.org/10.1177/13506501211059306
6. Zhou Q, Jacobson A (2016) Thingi10k: a dataset of 10,000 3d-printing models, arXiv preprint arXiv:1605.04797. 1–8. https://doi.org/10.48550/arXiv.1605.04797
7. Emery KJ, Parthasarathy MK, Joyce DS et al (2021) Color perception and compensation in color deficiencies assessed with hue scaling. Vis Res 183:1–15. https://doi.org/10.1016/j.visres.2021.01.006
8. Babaei V, Vidimče K, Foshey M et al (2017) Color contoning for 3D printing. ACM Trans Graph 36:1–15. https://doi.org/10.1145/3072959.3073605
9. Yuan J, Chen G, Li H et al (2021) Accurate and computational: a review of color reproduction in full-color 3D printing. 209:1–17. https://doi.org/10.1016/j.matdes.2021.109943
10. Cheng YL, Huang KC (2020) Preparation and characterization of color photocurable resins for full-color material jetting additive manufacturing. Polymers (Basel) 12:650. https://doi.org/10.3390/polym12030650
11. Wei X, Zou N, Zeng L et al (2022) PolyJet 3D printing: predicting color by multilayer perceptron neural network. Ann 3D Print Med 5:1–7. https://doi.org/10.1016/j.stlm.2022.100049
12. Stratasys (2018) PolyJet materials and uses: tips and tricks. https://grabcad.com/tutorials/polyjet-materials-and-uses-tips-and-tricks. Accessed 04 May 2022
13. Payami Golhin A, Strandlie A, John Green P (2021) The influence of wedge angle, feedstock color, and infill density on the color difference of FDM objects. J Imaging Sci Technol 65:1–15. https://doi.org/10.2352/J.ImagingSci.Technol.2021.65.5.050408
14. Spina R (2019) Performance analysis of colored PLA products with a fused filament fabrication process. Polymers (Basel) 11:1–16. https://doi.org/10.3390/polym11121984
15. Boulaala M, Elmessaoudi D, Buj-Corral I et al (2020) Towards design of mechanical part and electronic control of multi-material/multicolor fused deposition modeling 3D printing. Int J Adv Manuf Technol 110:45–55. https://doi.org/10.1007/s00170-020-05847-0
16. Wei X, Zeng L, Pei Z (2019) Experimental investigation of PolyJet 3D printing process: effects of finish type and material color on color appearance. ASME International Mechanical Engineering Congress and Exposition, Proceedings (IMECE). https://doi.org/10.1115/IMECE2019-11917
17. Zheng L, Li C, Yang S (2020) Analysis of color gamut in color 3D printing. In: Zhao P, Ye Z et al (eds) Lecture notes in electrical engineering. Springer, Singapore, pp 148–155. https://doi.org/10.1007/978-981-15-1864-5_21
18. Li C, Zheng L, Xiao Y (2020) Study on the influencing factors of color reproduction in color 3D printing. In: Zhao P, Ye Z et al (eds) Lecture notes in electrical engineering. Springer, Singapore, pp 156–163. https://doi.org/10.1007/978-981-15-1864-5_22
19. Arikan CA, Brunton A, Tanksale TM et al (2015) Color-managed 3D printing with highly translucent printing materials. Meas Model Reprod Mater Appear SPIE 2015. https://doi.org/10.1117/12.2083844
20. Elek O, Sumin D, Zhang R et al (2017) Scattering-aware texture reproduction for 3D printing. ACM Trans Graph 36:15. https://doi.org/10.1145/3130800.3130890
21. Brunton A, Arikan CA, Urban P (2015) Pushing the limits of 3D color printing: error diffusion with translucent materials. ACM Trans Graph 35:1–13. https://doi.org/10.1145/2832905
22. Brunton A, Arikan CA, Tanksale TM et al (2018) 3D printing spatially varying color and translucency. ACM Trans Graph 37:1–13. https://doi.org/10.1145/3197517.3201349
23. Wei X, Bhardwaj A, Zeng L et al (2021) Prediction and compensation of color deviation by response surface methodology for PolyJet 3d printing. J Manuf Mater Process 5(4):131. https://doi.org/10.3390/jmmp5040131
24. Kumar K, Kumar GS (2015) An experimental and theoretical investigation of surface roughness of poly-jet printed parts: this paper explains how local surface orientation affects surface roughness in a Poly-Jet process. Virtual Phys Prototyp 10:23–34. https://doi.org/10.1080/17452759.2014.999218
25. Gülcan O, Günaydın K, Çelik A (2022) Investigation on surface roughness of PolyJet-printed airfoil geometries for small UAV applications. Aerospace 9(2):82. https://doi.org/10.3390/aerospace9020082
26. Kim GD, Oh YT (2008) A benchmark study on rapid prototyping processes and machines: quantitative comparisons of mechanical properties, accuracy, roughness, speed, and material cost. Proc Inst Mech Eng B J Eng Manuf 222:201–215. https://doi.org/10.1243/09544054jem724
27. Zeng J, Deng H, Zhu Y et al (2021) Lenticular objects: 3D printed objects with lenticular lens surfaces that can change their appearance depending on the viewpoint. UIST 2021 - Proceedings of the 34th Annual ACM Symposium on User Interface Software and Technology. https://doi.org/10.1145/3472749.3474815
28. Elber G, Kim MS (2021) Synthesis of 3D jigsaw puzzles over freeform 2-manifolds. Comput Graph 102:339–348. https://doi.org/10.1016/j.cag.2021.10.014
29. Wang T, Si Y, Li N et al (2019) Bioinspired tip-guidance liquid jetting and droplet emission at a rotary disk via a surface energy gradient. ACS Nano 13:13100–13108. https://doi.org/10.1021/acsnano.9b05860
30. L'éclairage CID (2004) Colorimetry in CIE 015:2004. Commission Internationale de l'Éclairage. Vienna, Austria
31. Westland S, Ripamonti C, Cheung V (2012) Computational colour science using MATLAB. Wiley, West Sussex
32. Sharma G, Wu W, Dalal EN (2005) The CIEDE2000 color-difference formula: implementation notes, supplementary test data, and mathematical observations. Color Res Appl 30:21–30. https://doi.org/10.1002/col.20070
33. Klein GA, Meyrath T (2010) Industrial color physics. Springer, New York
34. Holmberg J, Berglund J, Wretland A et al (2019) Evaluation of surface integrity after high energy machining with EDM, laser beam machining and abrasive water jet machining of alloy 718. Int J Adv Manuf Technol 100:1575–1591. https://doi.org/10.1007/s00170-018-2697-z
35. Payami Golhin A (2021) Generation of micro-and nano-textured surfaces. European Commission. https://hdl.handle.net/11250/

2983515. Accessed 3 November 2022 https://doi.org/10.5281/zenodo.7293168
36. Hunt RWG, Pointer MR (2011) Measuring colour. Wiley, Chennai
37. Qiu T, Guo Y (2018) 10. Correlation estimation and power spectral density (PSD) estimation of random signals. In: Signal processing and data analysis. De Gruyter, pp 325–376. https://doi.org/10.1515/9783110465082-010
38. Barber J (2003) Bounds on the electrical resistance between contacting elastic rough bodies. Proc R Soc Lond A 459:53–66. https://doi.org/10.1098/rspa.2002.1038
39. Paggi M, Barber J (2011) Contact conductance of rough surfaces composed of modified RMD patches. Int J Heat Mass Transf 54:4664–4672. https://doi.org/10.1016/j.ijheatmasstransfer.2011.06.011
40. Yastrebov VA, Anciaux G, Molinari J-F (2015) From infinitesimal to full contact between rough surfaces: evolution of the contact area. Int J Solids Struct 52:83–102. https://doi.org/10.1016/j.ijsolstr.2014.09.019
41. ISO/TS 23031:2020(E) (2020) Graphic technology — assessment and validation of the performance of spectrocolorimeters and spectrodensitometers. International organization for standardization. Geneva, Switzerland. https://www.iso.org/standard/74361.html
42. Spearman C (1904) The proof and measurement of association between two things, In: Jenkins JJ, Paterson DG (eds) Studies in individual differences: the search for intelligence, Appleton-Century-Crofts, pp 45–58. https://doi.org/10.2307/1412159
43. Xia Y (2020) Chapter Eleven - Correlation and association analyses in microbiome study integrating multiomics in health and disease. In: Sun J (ed) Progress in molecular biology and translational science. Academic Press, pp 309–491. https://doi.org/10.1016/bs.pmbts.2020.04.003
44. Zuur AF, Ieno EN, Smith GM (2007) Principal component analysis and redundancy analysis. In: Analysing ecological data, 1st edn. Springer, New York, pp 193–224. https://doi.org/10.1007/978-0-387-45972-1_12
45. Olkkonen M, Hansen T, Gegenfurtner KR (2008) Color appearance of familiar objects: effects of object shape, texture, and illumination changes. J Vis 8:13–13. https://doi.org/10.1167/8.5.13
46. Bae JH, Hong KH, Lamar TM (2015) Effect of texture on color variation in inkjet-printed woven textiles. Color Res Appl 40:297–303
47. Sohaib A, Amano K, Xiao K et al (2018) Colour quality of facial prostheses in additive manufacturing. Int J Adv Manuf Technol 96:881–894. https://doi.org/10.1007/s00170-017-1480-x
48. Yan X, Yuan J, Chen G (2018) Applications analysis of paper-based color 3D printing in the map industry, In: Zhao P, Ye Z et al (eds) Lecture Notes in Electrical Engineering. Springer, Singapore, pp 377–383. https://doi.org/10.1007/978-981-10-7629-9_46
49. Cui M, Li X, Wu G et al (2019) Measurement and evaluation of the surface color of 3D paper product, In: Zhao P, Ye Z et al (eds) Lecture notes in electrical engineering. Springer, Singapore, pp 108–113. https://doi.org/10.1007/978-981-13-3663-8_16
50. Choudhury AKR (2014) Principles of colour and appearance measurement: object appearance, colour perception and instrumental measurement. Elsevier